UC Irvine
UC Irvine Previously Published Works

Title

Endoplasmic reticulum–associated degradation regulates mitochondrial dynamics in brown adipocytes

Permalink

https://escholarship.org/uc/item/3hx4z3xh

Journal

Science, 368(6486)

ISSN

0036-8075

Authors

Zhou, Zhangsen
Torres, Mauricio
Sha, Haibo
et al.

Publication Date

2020-04-03

DOI

10.1126/science.aay2494

Peer reviewed

Endoplasmic reticulum-associated degradation regulates mitochondrial dynamics in brown adipocytes

Zhangsen Zhou[1,†], Mauricio Torres[1,†], Haibo Sha[2,‡], Christopher J. Halbrook[1], Françoise Van den Bergh[1], Rachel B. Reinert[3], Tatsuya Yamada[4], Siwen Wang[1], Yingying Luo[1], Allen H. Hunter[5], Chunqing Wang[6], Thomas H. Sanderson[1,7], Meilian Liu[6], Aaron Taylor[8], Hiromi Sesaki[4], Costas A. Lyssiotis[1,9,10], Jun Wu[1,11], Sander Kersten[12], Daniel A. Beard[1], Ling Qi[1,3,*]

[1]Department of Molecular & Integrative Physiology, University of Michigan Medical School, Ann Arbor, MI 48105, USA; [2]Division of Nutritional Sciences, Cornell University, Ithaca, NY 14850, USA; [3]Department of Internal Medicine, Division of Metabolism, Endocrinology & Diabetes, University of Michigan Medical School, Ann Arbor, MI 48105, USA; [4]Department of Cell Biology, Johns Hopkins University School of Medicine, Baltimore, MD 21205, USA; [5]College of Engineering and Michigan Center for Materials Characterization, University of Michigan, Ann Arbor, MI 48109, USA; [6]Department of Biochemistry and Molecular Biology and Autophagy, Inflammation and Metabolism Center for Biomedical Research Excellence, University of New Mexico Health Sciences Center, Albuquerque, NM 87131, USA; [7]Department of Emergency Medicine, University of Michigan Medical School, Ann Arbor, MI 48105, USA; [8]Biomedical Research Core Facilities, University of Michigan, Ann Arbor, MI 48109, USA; [9]Department of Internal Medicine, Division of Gastroenterology and Hepatology, University of Michigan Medical School, Ann Arbor, MI 48105, USA; [10]Rogel Cancer Center, University of Michigan Medical School, Ann Arbor, MI 48105, USA; [11]Life Sciences Institute, University of Michigan, Ann Arbor, MI 48109, USA; [12]Nutrition Metabolism and Genomics group, Wageningen University, Wageningen, The Netherlands; [†]Contribute equally; [‡]Present address: In Vivo Pharmacology, Cardiovascular & Metabolic Diseases, Novartis Institutes for BioMedical Research, Inc., Cambridge, MA 02139, USA.

Abstract

The endoplasmic reticulum (ER) engages mitochondria at specialized ER domains known as mitochondria-associated membranes (MAMs). Here, we used three-dimensional high-resolution imaging to investigate the formation of pleomorphic "megamitochondria" with altered MAMs in brown adipocytes lacking the Sel1L-Hrd1 protein complex of ER-associated protein degradation (ERAD). Mice with ERAD deficiency in brown adipocytes were cold sensitive and exhibited mitochondrial dysfunction. ERAD deficiency affected ER-mitochondria contacts and mitochondrial dynamics, at least in part, by regulating the turnover of the MAM protein, sigma receptor 1 (SigmaR1). Thus, our study provides molecular insights into ER-mitochondrial crosstalk and expands our understanding of the physiological importance of Sel1L-Hrd1 ERAD.

One Sentence Summary:

This study reveals Sel1L-Hrd1 ERAD as a new regulatory mechanism underlying ER-mitochondrial communication in a physiological setting.

Membrane contact sites mediate interorganellar communication and are key to organelle homeostasis and organismal health (1–3). Endoplasmic reticulum (ER)-derived mitochondria-associated membranes (MAMs) are indispensable for mitochondrial dynamics and function. MAMs, characterized by intimate contact between the ER and mitochondria (~10–25 nm apart) (4), mark sites for mitochondrial DNA synthesis and fission (5–7), and for calcium exchange and lipid biosynthesis (1, 8, 9). During mitochondrial fission, ER tubules envelop and constrict mitochondria, and the activated dynamin-related GTPase protein (Drp1) aggregates to cleave the organelle (5, 10–13). The mechanism underlying interorganellar communication and physiological consequences of miscommunication remain largely unclear.

ER-associated degradation (ERAD) is a conserved quality control mechanism to recruit ER proteins for cytosolic proteasomal degradation (14–19). The Sel1L-Hrd1 protein complex comprises the most conserved form of ERAD from yeast to humans. Sel1L resides on the ER membrane and controls the stability of the E3 ligase Hrd1 (16–18, 20–22). Sel1L-Hrd1 ERAD is indispensable for fundamental physiological processes in vivo such as lipid metabolism, water balance, food intake, and systemic energy homeostasis (15, 19, 23–31).

Formation of megamitochondria in *Sel1L*$^{-/-}$ brown adipocytes

Serendipitously, we observed elongated mitochondria in *Sel1L*$^{-/-}$ primary brown preadipocytes, resembling those in *Drp1*$^{-/-}$ preadipocytes but distinct from those in pro-fusion *Opa1*$^{-/-}$ cells (Fig. S1A–B). These findings prompted us to explore a possible role of Sel1L in mitochondria-rich brown adipose tissue (BAT), a potential therapeutic target for obesity (32). Acute cold challenge induces mitochondrial fission in BAT to enhance respiration and maintain body temperature (33), while having no impact on the expression of ERAD genes (Fig. S2A–B).

We generated adipocyte-specific *Sel1L*-deficient mice (*Sel1L*^{AdipCre}) by crossing *Sel1L*$^{f/f}$ mice to the adiponectin promoter-driven Cre mice (25). Sel1L was deleted specifically in both white adipose tissue (WAT) and BAT, resulting in lower Hrd1 expression (Fig. S2C).

We next performed transmission electron microscopy (TEM) to visualize mitochondria in BAT from mice housed at room temperature (22°C), or 4°C for 6 hr. There was no difference in mitochondrial morphology between $Sel1L^{f/f}$ and $Sel1L^{AdipCre}$ BAT at 22°C (Fig. 1A–B). Acute cold challenge led to smaller mitochondria in $Sel1L^{f/f}$ BAT due to increased fission (Fig. 1A and 1C). By contrast, most mitochondria in $Sel1L^{AdipCre}$ brown adipocytes were enlarged and pleomorphic, with abnormal cristae architecture (yellow arrows, Fig. 1B–C and S3A–B). Consequently, mitochondrial density per cell was reduced in cold-stimulated $Sel1L^{AdipCre}$ mice compared to control (Fig. S3C).

To exclude a possible contribution from WAT, we generated brown adipocyte-specific $Sel1L$-deficient mice ($Sel1L^{Ucp1Cre}$) using Ucp1 promoter-driven Cre mice (Fig. S2D). Consistent with $Sel1L^{AdipCre}$ mice, mitochondria in $Sel1L^{Ucp1Cre}$ BAT were dramatically enlarged and pleomorphic upon acute cold exposure (yellow arrows, Fig. 1D–E and S3D). This observation was confirmed using confocal microscopy, with BAT immunolabeled for translocase of outer mitochondrial membrane 20 (Tomm20) and matrix protein pyruvate dehydrogenase (PDH) (Fig. S3E).

To gain further insight into mitochondrial morphology at the three-dimensional (3D) level, we performed serial block-face scanning electron microscopy (SBF-SEM) (Fig. S4A), which allows imaging of a large field (over 10 cells) at 3D planes with nanometer resolution (Fig. S4B–C) (34). In cold-exposed $Sel1L^{f/f}$ BAT, mitochondria were predominantly spherical or ovoid, with an average volume of ~1.7 μm^3 (Fig. S4B and 1F–H). Mitochondrial volume was increased five-fold in $Sel1L^{-/-}$ BAT (Fig. 1F–H and S4C). Moreover, three-dimensional reconstruction analyses revealed pleomorphic megamitochondria, e.g. branched, or chair- or cup-shaped (Fig. 1G and Movies S1–2). Thus, Sel1L deficiency in brown adipocytes triggers the formation of pleomorphic megamitochondria within hours of cold exposure.

Sel1L controls ER-mitochondria contacts

We next explored whether Sel1L deficiency affected MAMs. In $Sel1L^{f/f}$ BAT, MAMs were identified as thin sheets aligned with mitochondria, with the distance between the two organelles averaging 10–20 nm (cyan arrows, Fig. 2A, 2C–D and S5A). By contrast, MAMs of $Sel1L^{-/-}$ BAT formed tubules located closer to mitochondria, with an average distance of 5–10 nm (cyan arrows, Fig. 2B–D and S5B). Moreover, the number of MAMs per mitochondrion was increased in $Sel1L^{-/-}$ BAT following cold exposure (Fig. 2E). These peri-mitochondrial tubular structures were verified as ER by BiP-specific immunoelectron microscopy (Fig. 2F): pleomorphic megamitochondria appeared to "grow" around ER tubules in cold-stimulated $Sel1L^{-/-}$ BAT.

We next performed focused ion-beam SEM (FIB-SEM) to reconstruct mitochondria with MAMs at the 3D level. In comparison to SBF-SEM, FIB-SEM offers higher resolution at the z plane (35) with a resolution of 5 nm isotropic voxels (Fig. S6). Three-dimensional reconstruction revealed more intimate interactions between the ER (green) and mitochondria (purple) in $Sel1L^{Ucp1Cre}$ BAT vs. a $Sel1L^{f/f}$ mitochondria (pink) (Fig. 2G). In many U-shaped mitochondria, several ER tubules were found along the entire concavity of the organelle (orange arrows, Fig. 2G and Movie S3).

Formation of mitochondria-perforating ER tubules in the absence of Sel1L

In many U- or dumbbell-shaped megamitochondria, the outer membrane folded back on itself, with less than 10 nm between membranes (green arrows, Fig. 3A and S7A), which we speculated may fuse to embed ER tubules within the mitochondria. Indeed, there were many tubular structures embedded within mitochondrial profiles in $Sel1L^{-/-}$ BAT (red arrows, Fig. 3B–C, S7B–C). In some, double- or triple- membrane structures were noted. Moreover, these tubular structures served as a "hub" from which cristae folds radiated (Fig. 3B–C and S7B–D). To determine whether these peculiar structures inside mitochondria were ER, we performed BiP-specific immunoelectron microscopy. Clusters of BiP-positive signal were detected both perimitochondrially (cyan arrows) and within mitochondrial profiles (red arrows, Fig. 3D and S7E). We then performed SBF- and FIB-SEM to reconstruct whole mitochondria with perforating ER tubules. For example, we present 12 consecutive images of one megamitochondrion with two parallel penetrating ER tubules (Fig. S8 and 3E–F). Two ER tubules (arrows) perforated the mitochondrial profiles in parallel, with a distance of 1–1.3 μm apart, with radiating and interconnecting cristae folds, resembling wagon wheel spokes. Similarly, independent FIB-SEM analyses showed two parallel ER tubules (0.7–1 μm apart) penetrating another megamitochondrion in $Sel1L^{Ucp1Cre}$ BAT upon cold (Fig. S9 and Movie S4). Thus, Sel1L deficiency leads to the formation of pleomorphic megamitochondria with perforating ER tubule(s) in brown adipocytes upon cold challenge.

Impaired mitochondrial function and thermogenic response in $Sel1L^{-/-}$ mice

Next, we asked how Sel1L deficiency affected mitochondrial function and thermogenesis. Purified mitochondria from cold-exposed $Sel1L^{AdipCre}$ mice had reduced oxygen consumption rate (OCR) from oxidation of pyruvate and malate compared to those from $Sel1L^{f/f}$ mice (Fig. 4A). In addition, differentiated $Sel1L^{-/-}$ brown adipocytes showed defective respiration in response to adrenergic receptor agonist norepinephrine (NE) stimulation (Fig. 4B). Mitochondrial functional defects were further confirmed using a targeted metabolomics analysis of 119 intracellular metabolites in NE-treated differentiated $Sel1L^{f/f}$ vs. $Sel1L^{-/-}$ brown adipocytes (Fig. S10). Pathway analysis of the 30 significantly altered metabolites revealed three main pathways altered in $Sel1L^{-/-}$ adipocytes: TCA cycle, pyrimidine and purine metabolism (Fig. 4C), all of which are associated with mitochondrial function.

Both $Sel1L^{AdipCre}$ and $Sel1L^{Ucp1Cre}$ mice appeared normal and grew comparably to their $Sel1L^{f/f}$ littermates up to 22 weeks on low-fat diet at room temperature (Fig. S11A). While core body temperatures (~37°C) were similar between cohorts when housed at room temperature, $Sel1L^{AdipCre}$ mice were cold sensitive and dropped core body temperature to 26°C within 6 hr of cold exposure (Fig. 4D, vs. 33°C in $Sel1L^{f/f}$). Histological examination of BAT revealed that, while largely indistinguishable at room temperature, $Sel1L^{AdipCre}$ BAT exhibited larger lipid droplets upon cold exposure compared to $Sel1L^{f/f}$ mice (Fig. 4E), pointing to defects in lipid mobilization. This was confirmed using immunostaining of lipid droplet binding protein Perilipin 1 (Fig. 4F). Similar observations were made with $Sel1L^{Ucp1Cre}$ mice (Fig. 4D and S11B-C). Phosphorylation of hormone-sensitive lipase

(HSL) was not affected in response to β3-adrenergic receptor agonists (Fig. S11D–E), thereby uncoupling β-adrenergic signaling from the thermogenic defect of $Sel1L^{-/-}$ mice.

Sel1L effect on mitochondria is mediated through Hrd1 ERAD

Sel1L may have an Hrd1-independent function, and vice versa (25, 36, 37). To determine whether Sel1L and Hrd1 act similarly to regulate mitochondria in BAT, we generated brown adipocyte-specific $Hrd1$-deficient ($Hrd1^{Ucp1Cre}$) mice (Fig. S12A). Deletion of Hrd1 stabilized Sel1L protein (Fig. S12A), in line with the notion that Sel1L is a substrate of Hrd1. $Hrd1^{Ucp1Cre}$ mice grew normally (Fig. S12B), but were cold sensitive (Fig. 5A), with more lipid droplets in cold-challenged BAT compared to $Hrd1^{f/f}$ mice (Fig. S12C). Moreover, $Hrd1^{Ucp1Cre}$ BAT demonstrated enlarged mitochondrial, some with penetrating ER tubule(s), upon cold stimulation (Fig. 5B–D, S12D).

Because ER stress has been linked to mild mitochondrial elongation (38, 39), we next asked whether the effect of ERAD deficiency on mitochondria was mediated through ER stress. Basal $Xbp1$ mRNA splicing was slightly higher in $Sel1L^{AdipCre}$ BAT compared to $Sel1L^{f/f}$ BAT at room temperature; however, cold exposure reduced $Xbp1$ mRNA splicing in $Sel1L^{AdipCre}$ BAT (Fig. 5E). There was no detectable cell death in $Sel1L^{AdipCre}$ BAT (Fig. S13A). To study a possible impact of ER stress signaling on mitochondria in vivo, we generated mice lacking Ire1α, a key sensor of UPR, specifically in adipocytes ($Ire1a^{AdipCre}$). These knockout mice grew normally and were not cold-sensitive (Fig. S13B–D). Mitochondria from $Ire1a^{AdipCre}$ exhibited normal morphology, with reduced size at 4°C (Fig. 5F–G). Thus, the effect of Sel1L on mitochondria is mediated by ERAD, independent of ER stress or cell death.

Sel1L-Hrd1 ERAD regulates ER-mitochondria contacts and dynamics via SigmaR1

We next explored how mitochondrial dynamics were affected by ERAD dysfunction. While total protein levels of mitochondrial respiratory proteins and Ucp1 were largely comparable between the cohorts (Fig. S14A), cold-induced phosphorylation of Drp1 at Ser616, a key activating event in mitochondrial division (11, 40) was reduced in $Sel1L^{AdipCre}$ BAT compared to $Sel1L^{f/f}$ BAT (Fig. 6A). Opa1 processing to its shorter form upon cold exposure did not occur in $Sel1L^{AdipCre}$ BAT (Fig. 6A). Protein levels of outer mitochondrial membrane Drp1 receptors Fis1 and Mff were unchanged (Fig. S14A). Similar observations were obtained in $Hrd1^{-/-}$ BAT (Fig. S14B), but not in $Ire1a^{-/-}$ BAT (Fig. S13E). Furthermore, in $Sel1L^{-/-}$ BAT, cold exposure increased oligomerization of key fusion factor Mfn2 into high molecular weight (HMW) complexes as revealed by blue-native gels and sucrose gradient fractionation (Fig. S14C–D). Indeed, the Mfn2 HMW complex promotes mitochondrial fusion (41–43). We then tested the protein levels of several known MAM proteins including Mfn2, Vapb, Bap31 and SigmaR1. Only SigmaR1 levels were increased in $Sel1L$- and $Hrd1$-deficient BAT (Fig. 6B and S15A–B), but not in $Ire1a^{-/-}$ BAT (Fig. S13E). However, $SigmaR1$ mRNA level was comparable in $Sel1L^{-/-}$ vs. WT BAT in response to cold (Fig. S15C), pointing to a post-transcriptional regulation of SigmaR1 protein.

SigmaR1 is a single-span ER-resident protein residing at the MAMs where it may regulate ER-mitochondria contacts and mitochondrial dynamics (44, 45), although a detailed mechanism remains vague. SigmaR1 protein was degraded by the proteasome with a half-life of approximately 6 hr (Fig. 6C), interacted with the E3 ligase Hrd1 (Fig. S15D–E) and was ubiquitinated in a largely Hrd1-dependent manner (Fig. 6D). In the absence of Sel1L or Hrd1, SigmaR1 protein was stabilized (Fig. 6C) and accumulated in the ER (Fig. S15F). SigmaR1 interacted with Mfn2 as well as other MAM proteins Bap31 and Vapb, but not Ip3r (Fig. 6E and S15G), and were localized at very close proximity to mitochondria in $Sel1L^{-/-}$ cells (Fig. S16H). Genetic deletion of $SigmaR1$ reduced cold-induced Mfn2 HMW complexes in $Sel1L^{-/-}$ brown adipocytes (Fig. 6F and S16A). Deletion of $SigmaR1$ reversed mitochondrial elongation (Fig. S16B–C) and reduced ER-mitochondrial contacts in $Sel1L^{-/-}$ cells (Fig. 6G–H). In a mitochondrial fusion assay (33) using mitochondria-targeted photoactivated GFP (mito-PAGFP), deletion of $SigmaR1$ attenuated the spread and decay of GFP intensity seen in $Sel1L^{-/-}$ brown adipocytes upon NE treatment (Fig. 6I–J). Thus, SigmaR1 mediates mitochondrial hyperfusion in $Sel1L$-deficient cells, thereby linking ERAD to ER-mitochondrial contacts and mitochondrial dynamics in brown adipocytes.

Discussion

Here, we found a critical role for Sel1L-Hrd1 ERAD in regulating ER-mitochondria contacts and mitochondrial function. We observed profound changes in mitochondrial morphology, beyond mere elongation or swelling that is commonly associated with mitochondrial dysfunction or ER stress. Using 3D imaging techniques, we reconstructed these pleomorphic mitochondria and their associated MAMs. We speculate that the ER tubules embedded within profiles of pleomorphic megamitochondria represent halted fission and/or accelerated fusion intermediates. Our mechanistic studies identified MAM protein SigmaR1 as an ERAD substrate, which, when deleted, reduced ER-mitochondria contacts and rescued abnormal mitochondrial dynamics and morphology in $Sel1L^{-/-}$ cells. SigmaR1 may regulate mitochondrial dynamics by interacting with Mfn2 as well as other MAM proteins and promoting Mfn2 oligomerization in an unknown manner.

MAMs are disturbed in many diseases such as obesity (46), cardiac disease (47), and neurodegeneration (48); however, to date, the nature of this disruption in disease pathogenesis remains vague. Our data suggest that Sel1L-Hrd1 ERAD may regulate the dynamics of ER-mitochondria interactions via modulation of MAMs. Indeed, an inverse correlation between Sel1L and SigmaR1 expression levels has been reported in patients with neurodegeneration (49–51). Considering the recent identification of Sel1L mutants in progressive early-onset cerebellar ataxia in canines (52) and various cancers (53, 54), this study may have implications not only for interorganelle communication, but also for the pathophysiological role of Sel1L-Hrd1 ERAD.

Supplementary Material

Refer to Web version on PubMed Central for supplementary material.

ACKNOWLEDGEMENT

REFERENCES AND NOTES

1. Wu H, Carvalho P, Voeltz GK, Here, there, and everywhere: The importance of ER membrane contact sites. Science 361, (2018).

2. Rowland AA, Voeltz GK, Endoplasmic reticulum-mitochondria contacts: function of the junction. Nat Rev Mol Cell Biol 13, 607–625 (2012). [PubMed: 22992592]

3. Kornmann B et al., An ER-mitochondria tethering complex revealed by a synthetic biology screen. Science 325, 477–481 (2009). [PubMed: 19556461]

4. Csordas G et al., Structural and functional features and significance of the physical linkage between ER and mitochondria. J Cell Biol 174, 915–921 (2006). [PubMed: 16982799]

5. Friedman JR et al., ER tubules mark sites of mitochondrial division. Science 334, 358–362 (2011). [PubMed: 21885730]

6. Murley A et al., ER-associated mitochondrial division links the distribution of mitochondria and mitochondrial DNA in yeast. eLife 2, e00422 (2013). [PubMed: 23682313]

7. Lewis SC, Uchiyama LF, Nunnari J, ER-mitochondria contacts couple mtDNA synthesis with mitochondrial division in human cells. Science 353, aaf5549 (2016). [PubMed: 27418514]

8. Salvador-Gallego R, Hoyer MJ, Voeltz GK, SnapShot: Functions of Endoplasmic Reticulum Membrane Contact Sites. Cell 171, 1224–1224 e1221 (2017). [PubMed: 29149609]

9. Lee KS et al., Altered ER-mitochondria contact impacts mitochondria calcium homeostasis and contributes to neurodegeneration in vivo in disease models. Proc Natl Acad Sci U S A 115, E8844–E8853 (2018). [PubMed: 30185553]

10. Ji WK et al., Receptor-mediated Drp1 oligomerization on endoplasmic reticulum. J Cell Biol 216, 4123–4139 (2017). [PubMed: 29158231]

11. Smirnova E, Griparic L, Shurland DL, van der Bliek AM, Dynamin-related protein Drp1 is required for mitochondrial division in mammalian cells. Mol Biol Cell 12, 2245–2256 (2001). [PubMed: 11514614]

12. Labrousse AM, Zappaterra MD, Rube DA, van der Bliek AM, elegans C dynamin-related protein DRP-1 controls severing of the mitochondrial outer membrane. Mol Cell 4, 815–826 (1999). [PubMed: 10619028]

13. Bleazard W et al., The dynamin-related GTPase Dnm1 regulates mitochondrial fission in yeast. Nat Cell Biol 1, 298–304 (1999). [PubMed: 10559943]

14. Hwang J, Qi L, Quality Control in the Endoplasmic Reticulum: Crosstalk between ERAD and UPR pathways. Trends Biochem Sci 43, 593–605 (2018). [PubMed: 30056836]

15. Qi L, Tsai B, Arvan P, New Insights into the Physiological Role of Endoplasmic Reticulum-Associated Degradation. Trends Cell Biol 27, 430–440 (2017). [PubMed: 28131647]

16. Carvalho P, Goder V, Rapoport TA, Distinct ubiquitin-ligase complexes define convergent pathways for the degradation of ER proteins. Cell 126, 361–373 (2006). [PubMed: 16873066]

17. Gardner RG et al., Endoplasmic reticulum degradation requires lumen to cytosol signaling. Transmembrane control of Hrd1p by Hrd3p. J Cell Biol 151, 69–82 (2000). [PubMed: 11018054]

18. Hampton RY, Gardner RG, Rine J, Role of 26S proteasome and HRD genes in the degradation of 3-hydroxy-3-methylglutaryl-CoA reductase, an integral endoplasmic reticulum membrane protein. Mol Biol Cell 7, 2029–2044 (1996). [PubMed: 8970163]

19. Bhattacharya A, Qi L, ER-associated degradation in health and disease - from substrate to organism. J Cell Sci 132, (2019).

20. Vashistha N, Neal SE, Singh A, Carroll SM, Hampton RY, Direct and essential function for Hrd3 in ER-associated degradation. Proc Natl Acad Sci U S A 113, 5934–5939 (2016). [PubMed: 27170191]

21. Wu X, Rapoport TA, Mechanistic insights into ER-associated protein degradation. Curr Opin Cell Biol 53, 22–28 (2018). [PubMed: 29719269]

22. Schoebel S et al., Cryo-EM structure of the protein-conducting ERAD channel Hrd1 in complex with Hrd3. Nature 548, 352–355 (2017). [PubMed: 28682307]

23. Kim GH et al., Hypothalamic ER-associated degradation regulates POMC maturation, feeding and age-associated obesity. J Clin Invest 128, 1125–1140 (2018). [PubMed: 29457782]

24. Shi G et al., ER-associated degradation is required for vasopressin prohormone processing and systemic water homeostasis. J Clin Invest 127, 3897–3912 (2017). [PubMed: 28920920]

25. Sha H et al., The ER-associated degradation adaptor protein Sel1L regulates LPL secretion and lipid metabolism. Cell Metab 20, 458–470 (2014). [PubMed: 25066055]

26. Sun S et al., Sel1L is indispensable for mammalian endoplasmic reticulum-associated degradation, endoplasmic reticulum homeostasis, and survival. Proc Natl Acad Sci U S A 111, E582–591 (2014). [PubMed: 24453213]

27. Bhattacharya A et al., Hepatic Sel1L-Hrd1 ER-associated degradation (ERAD) manages FGF21 levels and systemic metabolism via CREBH. EMBO J 37, e99277 (2018). [PubMed: 30389665]

28. Ji Y et al., The Sel1L-Hrd1 Endoplasmic Reticulum-Associated Degradation Complex Manages a Key Checkpoint in B Cell Development. Cell reports 16, 2630–2640 (2016). [PubMed: 27568564]

29. Yang Y et al., The endoplasmic reticulum-resident E3 ubiquitin ligase Hrd1 controls a critical checkpoint in B cell development in mice. J Biol Chem 293, 12934–12944 (2018). [PubMed: 29907570]

30. Wei J et al., HRD1-ERAD controls production of the hepatokine FGF21 through CREBH polyubiquitination. EMBO J 37, e98942 (2018). [PubMed: 30389664]

31. Sun S et al., Epithelial Sel1L is required for the maintenance of intestinal homeostasis. Mol Biol Cell 27, 483–490 (2016). [PubMed: 26631554]

32. Cypess AM, Kahn CR, Brown fat as a therapy for obesity and diabetes. Current opinion in endocrinology, diabetes, and obesity 17, 143–149 (2010).

33. Wikstrom JD et al., Hormone-induced mitochondrial fission is utilized by brown adipocytes as an amplification pathway for energy expenditure. EMBO J 33, 418–436 (2014). [PubMed: 24431221]

34. Denk W, Horstmann H, Serial block-face scanning electron microscopy to reconstruct three-dimensional tissue nanostructure. PLoS Biol 2, e329 (2004). [PubMed: 15514700]

35. Knott G, Marchman H, Wall D, Lich B, Serial section scanning electron microscopy of adult brain tissue using focused ion beam milling. J Neurosci 28, 2959–2964 (2008). [PubMed: 18353998]

36. Schulz J et al., Conserved cytoplasmic domains promote Hrd1 ubiquitin ligase complex formation for ER-associated degradation (ERAD). J Cell Sci 130, 3322–3335 (2017). [PubMed: 28827405]

37. Christianson JC et al., Defining human ERAD networks through an integrative mapping strategy. Nat Cell Biol 14, 93–105 (2012).

38. Balsa E et al., ER and Nutrient Stress Promote Assembly of Respiratory Chain Supercomplexes through the PERK-eIF2alpha Axis. Mol Cell, doi: 10.1016/j.molcel.2019.1003.1031. (2019).

39. Lebeau J et al., The PERK Arm of the Unfolded Protein Response Regulates Mitochondrial Morphology during Acute Endoplasmic Reticulum Stress. Cell reports 22, 2827–2836 (2018). [PubMed: 29539413]

40. Smirnova E, Shurland DL, Ryazantsev SN, van der Bliek AM, A human dynamin-related protein controls the distribution of mitochondria. J Cell Biol 143, 351–358 (1998). [PubMed: 9786947]

41. Steffen J et al., Rapid degradation of mutant SLC25A46 by the ubiquitin-proteasome system results in MFN1/2-mediated hyperfusion of mitochondria. Mol Biol Cell 28, 600–612 (2017). [PubMed: 28057766]

42. McLelland GL et al., Mfn2 ubiquitination by PINK1/parkin gates the p97-dependent release of ER from mitochondria to drive mitophagy. eLife 7, (2018).

43. Sugiura A et al., MITOL regulates endoplasmic reticulum-mitochondria contacts via Mitofusin2. Mol Cell 51, 20–34 (2013). [PubMed: 23727017]

44. Gregianin E et al., Loss-of-function mutations in the SIGMAR1 gene cause distal hereditary motor neuropathy by impairing ER-mitochondria tethering and Ca2+ signalling. Hum Mol Genet 25, 3741–3753 (2016). [PubMed: 27402882]

45. Bernard-Marissal N, Medard JJ, Azzedine H, Chrast R, Dysfunction in endoplasmic reticulum-mitochondria crosstalk underlies SIGMAR1 loss of function mediated motor neuron degeneration. Brain 138, 875–890 (2015). [PubMed: 25678561]

46. Arruda AP et al., Chronic enrichment of hepatic endoplasmic reticulum-mitochondria contact leads to mitochondrial dysfunction in obesity. Nat Med 20, 1427–1435 (2014). [PubMed: 25419710]

47. Zhou H, Wang S, Hu S, Chen Y, Ren J, ER-Mitochondria Microdomains in Cardiac Ischemia-Reperfusion Injury: A Fresh Perspective. Front Physiol 9, 755 (2018). [PubMed: 29962971]

48. Paillusson S et al., There's Something Wrong with my MAM; the ER-Mitochondria Axis and Neurodegenerative Diseases. Trends Neurosci 39, 146–157 (2016). [PubMed: 26899735]

49. Montibeller L, de Belleroche J, Amyotrophic lateral sclerosis (ALS) and Alzheimer's disease (AD) are characterised by differential activation of ER stress pathways: focus on UPR target genes. Cell Stress Chaperones 23, 897–912 (2018). [PubMed: 29725981]

50. Prause J et al., Altered localization, abnormal modification and loss of function of Sigma receptor-1 in amyotrophic lateral sclerosis. Hum Mol Genet 22, 1581–1600 (2013). [PubMed: 23314020]

51. Mori T, Hayashi T, Su TP, Compromising sigma-1 receptors at the endoplasmic reticulum render cytotoxicity to physiologically relevant concentrations of dopamine in a nuclear factor-kappaB/Bcl-2-dependent mechanism: potential relevance to Parkinson's disease. J Pharmacol Exp Ther 341, 663–671 (2012). [PubMed: 22399814]

52. Kyostila K et al., A SEL1L mutation links a canine progressive early-onset cerebellar ataxia to the endoplasmic reticulum-associated protein degradation (ERAD) machinery. PLoS Genet 8, e1002759 (2012). [PubMed: 22719266]

53. Kim H, Bhattacharya A, Qi L, Endoplasmic reticulum quality control in cancer: Friend or foe. Semin Cancer Biol 33, 25–33 (2015). [PubMed: 25794824]

54. Mellai M et al., SEL1L SNP rs12435998, a predictor of glioblastoma survival and response to radio-chemotherapy. Oncotarget 6, 12452–12467 (2015). [PubMed: 25948789]

55. Wu T et al., Hrd1 suppresses Nrf2-mediated cellular protection during liver cirrhosis. Genes Dev 28, 708–722 (2014). [PubMed: 24636985]

56. Iwawaki T, Akai R, Yamanaka S, Kohno K, Function of IRE1 alpha in the placenta is essential for placental development and embryonic viability. Proc Natl Acad Sci USA 106, 16657–16662 (2009). [PubMed: 19805353]

57. Eguchi J et al., Transcriptional control of adipose lipid handling by IRF4. Cell Metab 13, 249–259 (2011). [PubMed: 21356515]

58. Yamada T et al., Mitochondrial Stasis Reveals p62-Mediated Ubiquitination in Parkin-Independent Mitophagy and Mitigates Nonalcoholic Fatty Liver Disease. Cell Metab 28, 588–604 e585 (2018). [PubMed: 30017357]

59. Wittig I, Braun HP, Schägger H, Blue native PAGE. Nat Protoc 1, 418–428 (2006). [PubMed: 17406264]

60. Sun S, Xia S, Ji Y, Kersten S, Qi L, The ATP-P2X7 Signaling Axis Is Dispensable for Obesity-Associated Inflammasome Activation in Adipose Tissue. Diabetes 61, 1471–1478 (2012). [PubMed: 22415881]

61. Kikkert M et al., Human HRD1 is an E3 ubiquitin ligase involved in degradation of proteins from the endoplasmic reticulum. J Biol Chem 279, 3525–3534 (2004). [PubMed: 14593114]

62. Klein J, Fasshauer M, Klein HH, Benito M, Kahn CR, Novel adipocyte lines from brown fat: a model system for the study of differentiation, energy metabolism, and insulin action. Bioessays 24, 382–388 (2002). [PubMed: 11948624]

63. Twig G et al., Tagging and tracking individual networks within a complex mitochondrial web with photoactivatable GFP. American journal of physiology. Cell physiology 291, C176–184 (2006). [PubMed: 16481372]

64. Pike JA, Styles IB, Rappoport JZ, Heath JK, Quantifying receptor trafficking and colocalization with confocal microscopy. Methods 115, 42–54 (2017). [PubMed: 28131869]
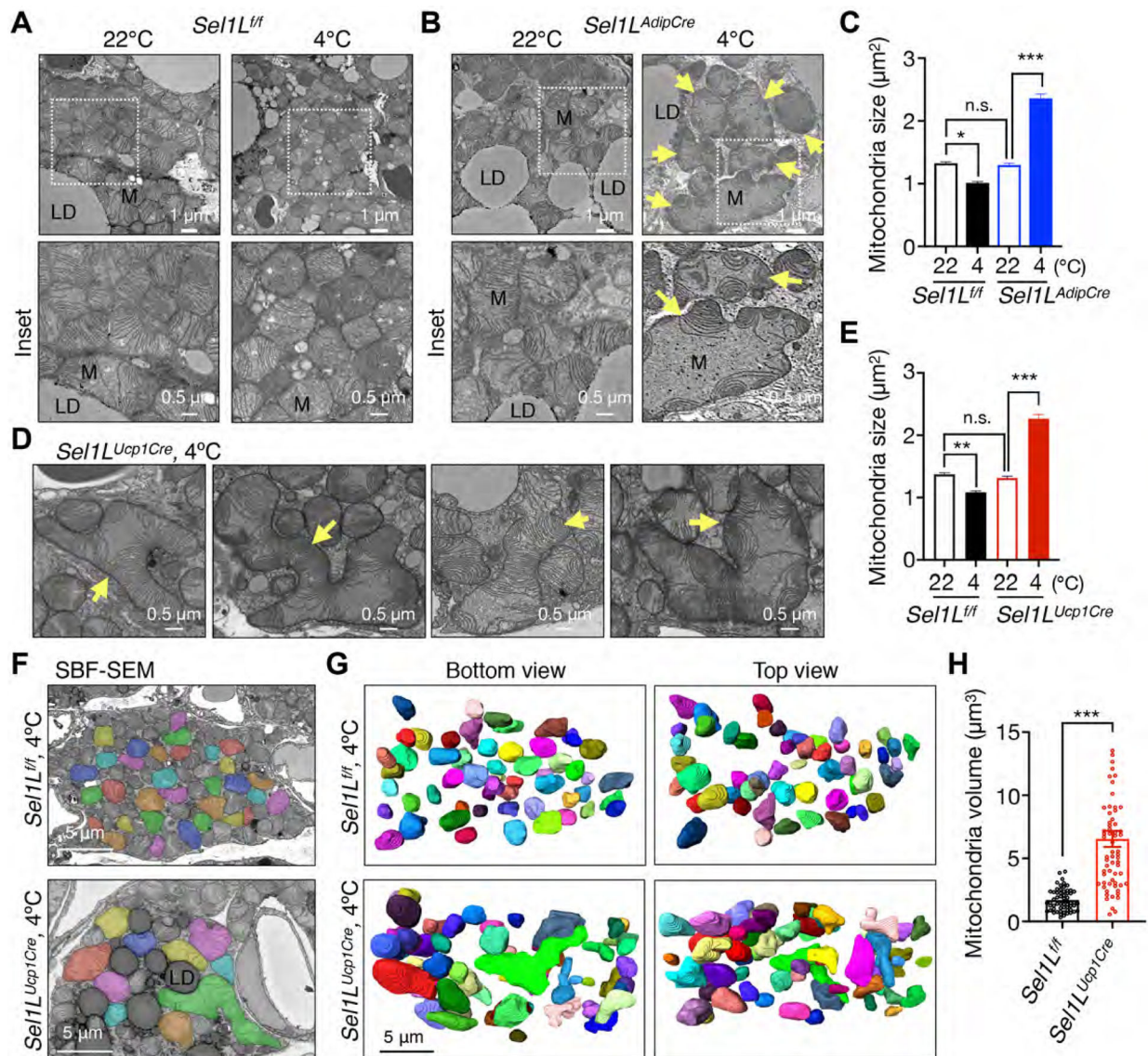
Figure 1. Sel1L regulates mitochondrial morphology in BAT during cold exposure.
(A-C) Representative TEM images of BAT from *Sel1L^f/f* (A) and *Sel1L^AdipCre* mice (B) at 22°C (left) or 4°C (right) for 6 hr, with quantitation of mitochondrial size shown in C (n=870, 601 mitochondria from 3 *Sel1L^f/f* mice each at 22°C and 4°C; 624, 821 from 3 *Sel1L^AdipCre* mice each at 22°C and 4°C, one-way ANOVA). Yellow arrows, megamitochondria. M, mitochondrion; LD, lipid droplet. (D-E) Representative TEM images of BAT from *Sel1L^Ucp1Cre* mice at 4°C for 6 hr, with quantitation of mitochondrial size shown in E (n=676, 618 mitochondria for 3 *Sel1L^f/f* mice each at 22°C and 4°C; 582, 674 for 3 *Sel1L^Ucp1Cre* mice each at 22°C and 4°C, one-way ANOVA). (F-H) Representative SBF-SEM images (F) and 3D reconstruction (G) of mitochondria from BAT of *Sel1L^f/f* and *Sel1L^Ucp1Cre* mice at 4°C for 6 hr. Mitochondria in pseudo colors were reconstructed from a set of 150 SBF-SEM image stacks (65 nm/slice). (H) Quantitation of 3D volume of mitochondria (n=61 and 63, *Sel1L^f/f* and *Sel1L^Ucp1Cre* mice, Student's *t*-test). All
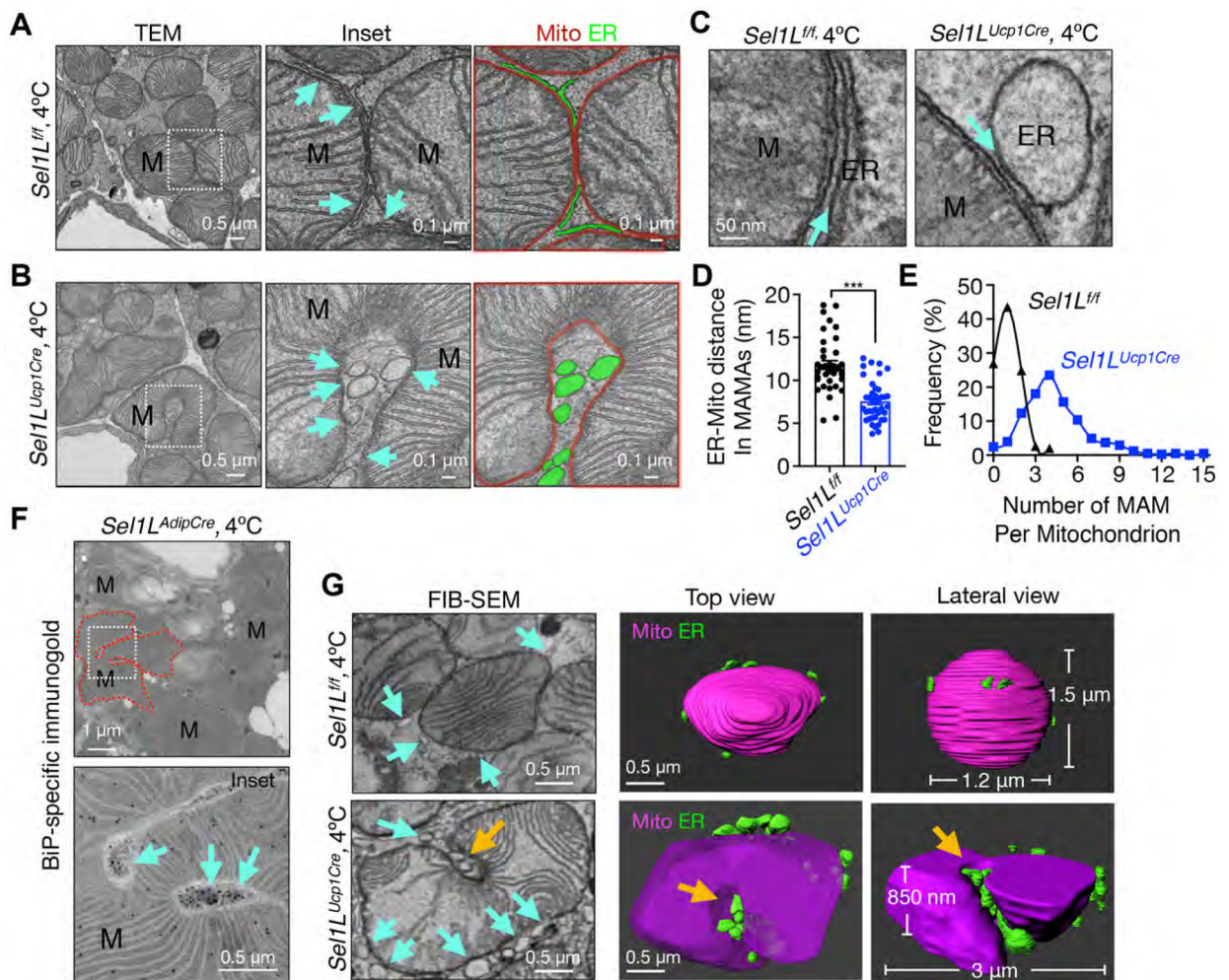
experiments have been repeated three times. Data are mean ± SEM. *, p< 0.05; **, p< 0.01; ***, p< 0.001; n.s., not significant.

Figure 2. Sel1L controls ER-mitochondria contacts in cold-stimulated brown adipocytes.
(A-B) Representative TEM images of BAT from *Sel1L^{f/f}* (A) and *Sel1L^{Ucp1Cre}* (B) mice at 4°C for 6 hr. M, mitochondrion; Cyan arrows, MAMs; red lines, mitochondrial membranes; the ER, green. (C-E) Representative TEM images of the MAMs in BAT from *Sel1L^{f/f}* and *Sel1L^{Ucp1Cre}* mice at 4°C for 6 hr, with quantitation of ER-mitochondrion distance (D) and abundance of MAM per mitochondrion (E). n=35 and 40 MAMs (D) and n=450 and 572 mitochondria (E) for *Sel1L^{f/f}* and *Sel1L^{Ucp1Cre}*. (F) Representative TEM images of BiP-specific immunogold labeling in BAT from *Sel1L^{AdipCre}* mice at 4°C for 6 hr. Red dotted line outlines one megamitochondrion; cyan arrows, BiP-positive ER tubule(s). (G) Representative FIB-SEM (left) and the 3D tomography images (300 and 170 slices, 5 nm/slice) of mitochondria in BAT from *Sel1L^{f/f}* and *Sel1L^{Ucp1Cre}* mice at 4°C for 6 hr. Magenta, mitochondria; green, ER. Cyan arrows, MAMs; orange arrows, MAMs going through the concave surface of a mitochondrion. All experiments have been repeated two to three times. Data are mean ± SEM. ***, p< 0.001 by Student's *t*-test.
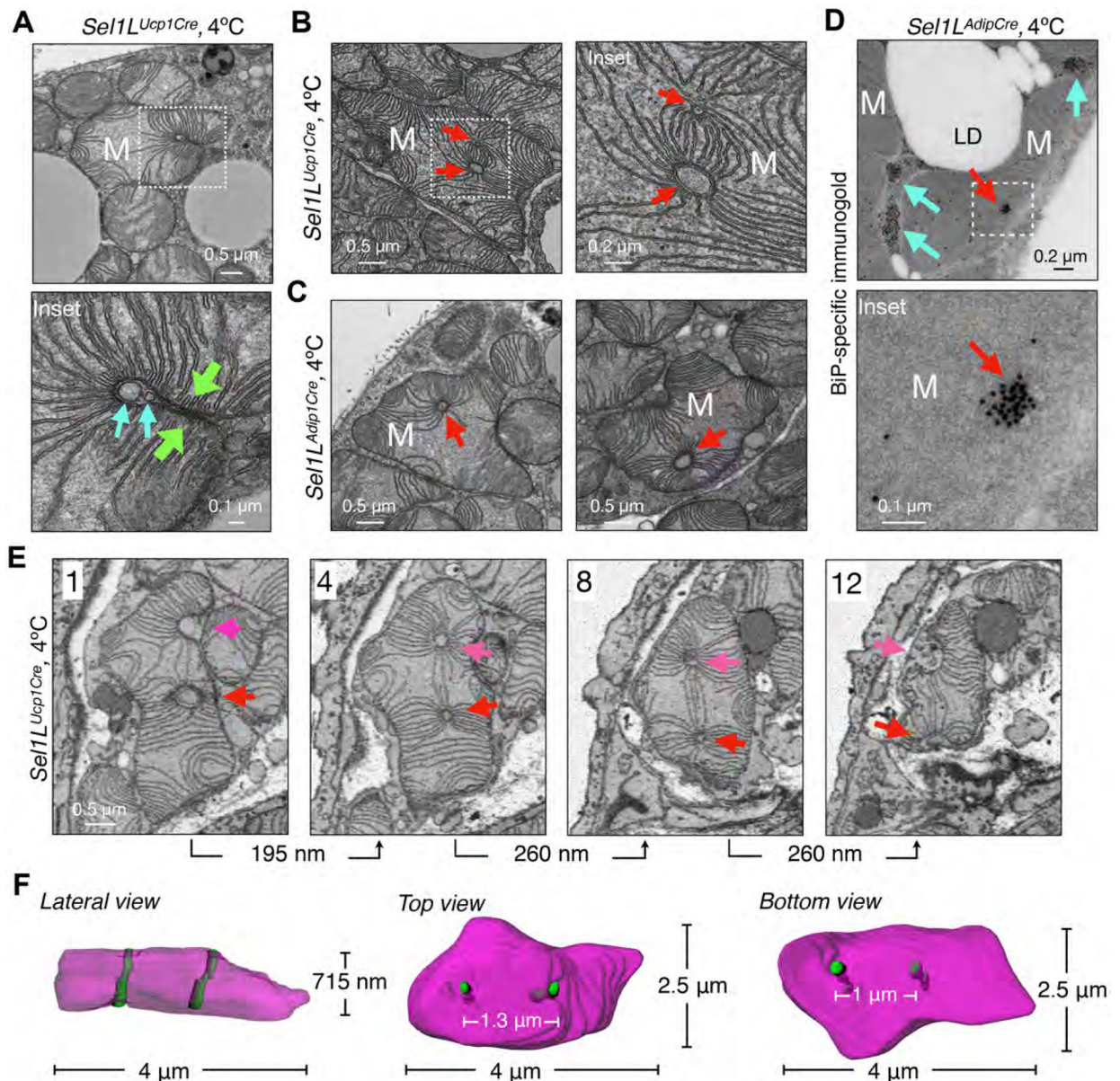
Figure 3. Sel1L deficiency leads to the formation of megamitochondria with perforating ER tubules.

(A) Representative TEM images of BAT in $Sel1L^{Ucp1Cre}$ mice housed at 4°C for 6 hr, showing a megamitochondrion wrapping around the tubular structures (cyan arrows). Green arrows, two opposite sides of a mitochondrion. (B-C) Representative TEM images of BAT from $Sel1L^{Ucp1Cre}$ (B) and $Sel1L^{AdipCre}$ (C) mice at 4°C for 6 hr, showing megamitochondria with tubular structures (red arrows). (D) Representative BiP-immunogold TEM images of BAT in $Sel1L^{AdipCre}$ mice at 4°C for 6 hr. Red and cyan arrows, mitochondria-perforating ER tubules and peri-mitochondria ER tubules. (E-F) Representative SBF-SEM images (E) and 3D reconstruction (F) in BAT of $Sel1L^{Ucp1Cre}$ mice at 4°C for 6 hr, showing four different slices of a megamitochondrion with two parallel

perforating ER tubules (red and magenta arrows). All 12 slices (65 nm/slice) are shown in Fig. S8. All experiments have been repeated two to three times.
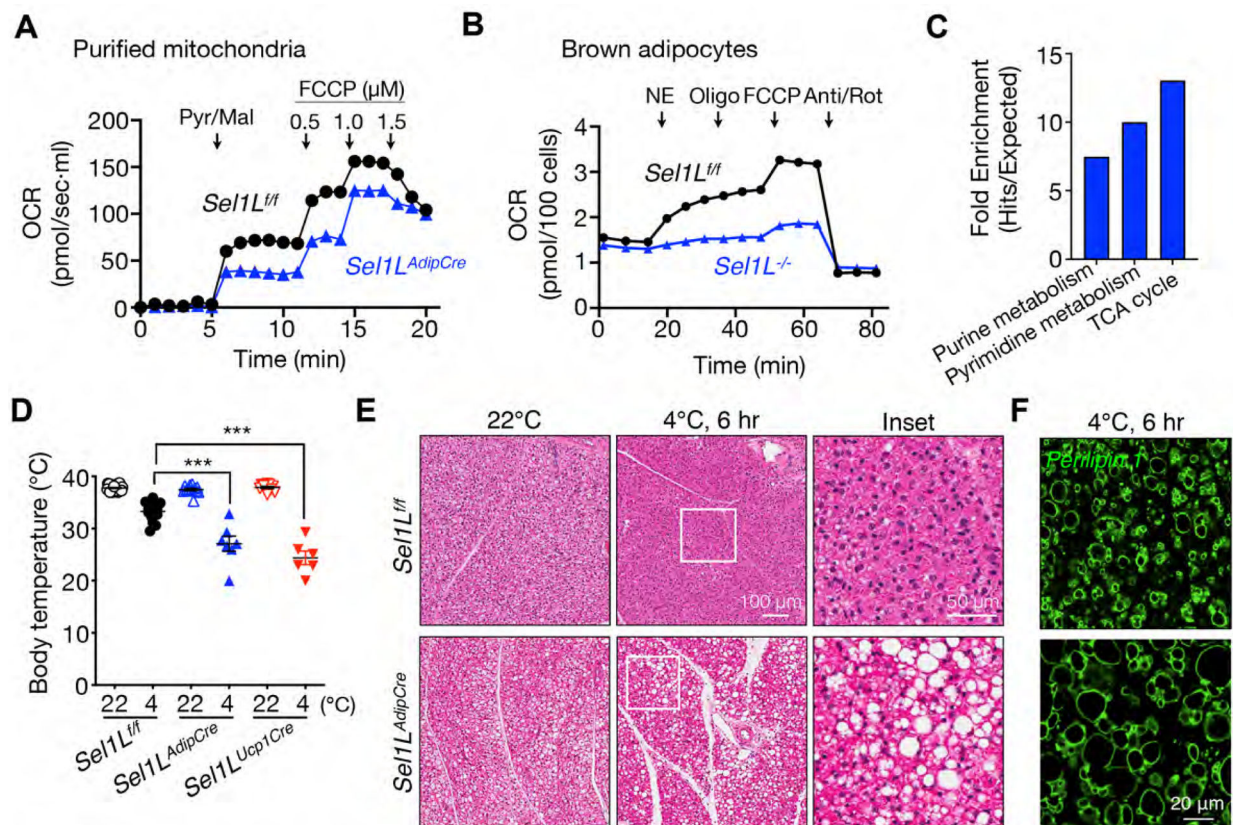
Figure 4. Sel1L in brown adipocytes regulates mitochondrial function and cold-induced thermogenesis.

(A-B) Oxygen consumption rate (OCR) of purified mitochondria from BAT of cold-exposed mice (A) and differentiated brown adipocytes (B) with the addition of various stimuli as indicated. NE, norepinephrine; Oligo, oligomycin; Pyr/Mal, pyruvate/malate; FCCP, carbonyl cyanide p-trifluoromethoxyphenylhydrazone; Anti, antimycin; Rot, Rotenone. (C) Metaboanalyst pathway enrichment analysis for the metabolites in $Sel1L^{f/f}$ and $Sel1L^{-/-}$ brown adipocytes treated with 1 μM NE for 1 hr (n=3/group). (D) Rectal temperature of 8- to 10- week-old mice housed at 22°C or 4°C for 6 hr (n=7–10 mice each, one-way ANOVA). (E-F) Representative H&E (E) and Perilipin1 (F) staining of BAT from $Sel1L^{f/f}$ and $Sel1L^{AdipCre}$ mice housed at 22°C or 4°C for 6 hr. All experiments have been repeated three times except panel C (3 samples per group). Data are mean ± SEM. ***, p< 0.001.
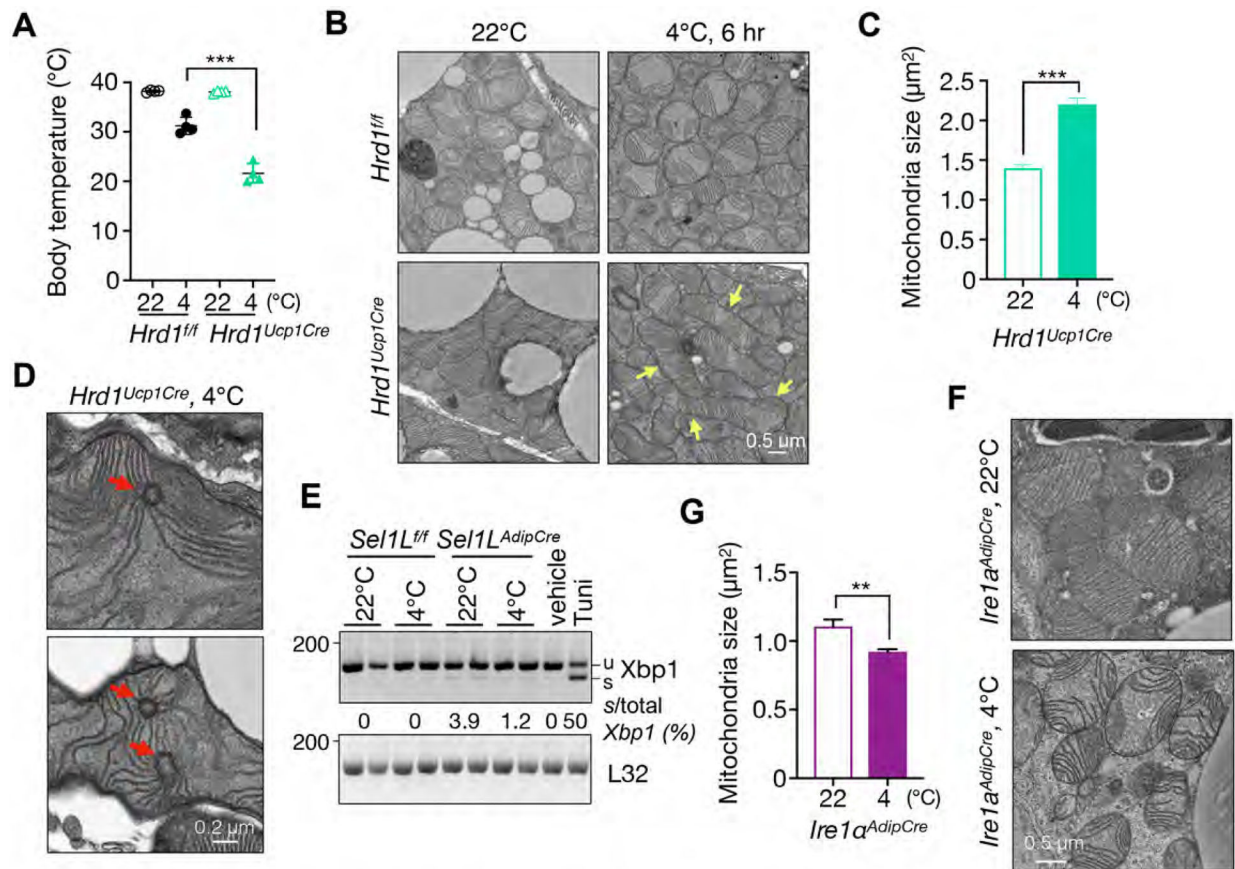
Figure 5. Hrd1, but not Ire1α of UPR, controls mitochondrial morphology and thermogenesis in brown adipocytes.

(A) Rectal temperature of 8- to 10- week-old *Hrd1^f/f* and *Hrd1^Ucp1Cre* mice housed at 22°C or 4°C for 6 hr, n=4/group (one-way ANOVA). (B-D) Representative TEM images of BAT from *Hrd1^f/f* and *Hrd1^Ucp1Cre* mice housed at 22°C or 4°C for 6 hr with quantitation shown in C. n= 543, 581 mitochondria for 22°C and 4°C, Student's *t*-test. Yellow arrows, megamitochondria; red arrows, ER tubules within mitochondrial profiles. (E) RT-PCR analysis of *Xbp1* mRNA splicing in BAT at 22°C or 4°C for 6 hr with quantitation of the ratio of spliced Xbp1 (s) to total Xbp1 (spliced + unspliced (u)) shown below the gel (n = 6 mice per group). BAT from wildtype mice injected with vehicle or tunicamycin (Tuni, 1 mg/kg) included as controls. (F-G) Representative TEM pictures of BAT from *Ire1a^AdipCre* mice at 4°C for 6 hr with quantitation shown in G (n=500, 665 from 2 mice each, Student's *t*-test). All experiments have been repeated two to three times. Data are mean ± SEM. **, p< 0.01; ***, p< 0.001.
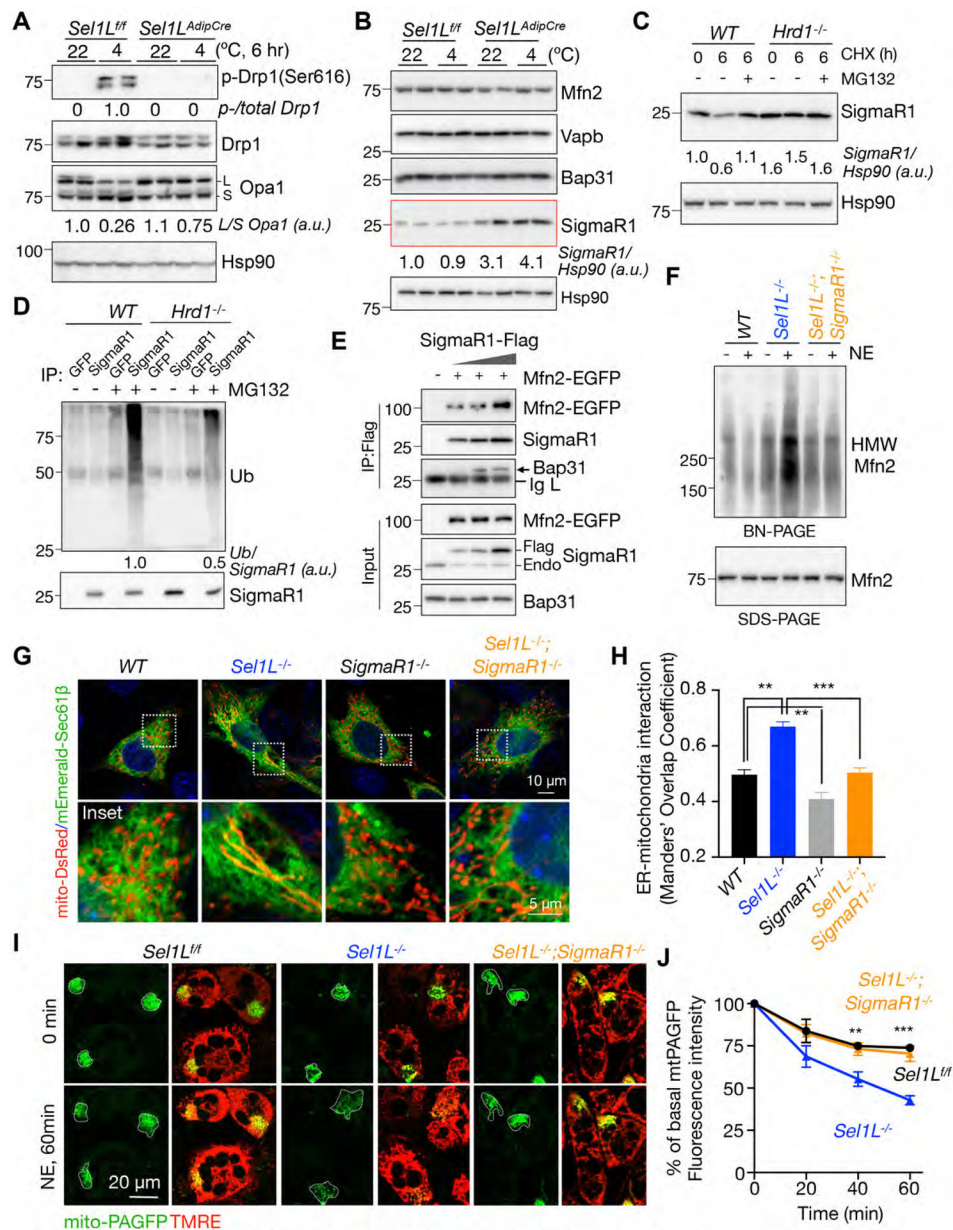
Figure 6. Sel1L-Hrd1 ERAD regulates MAM and mitochondrial dynamics via SigmaR1.
(A) Immunoblot analysis of mitochondrial dynamic proteins in BAT from *Sel1L^{f/f}* and *Sel1L^{AdipCre}* mice at 22°C or 4°C for 6 hr with quantitation of phos-/total Drp1 and large (L)-/small (S)-Opa1 shown below the gel (n = 7 per group). (B) Immunoblot analysis of MAM proteins in BAT of *Sel1L^{f/f}* and *Sel1L^{AdipCre}* mice with quantitation of SigmaR1/ Hsp90 shown below the gel (n = 7 per group). (C) Immunoblot analysis of endogenous SigmaR1 in *WT* and *Hrd1*-deficient (*Hrd1^{−/−}*) HEK293T cells with or without CHX and MG132 treatment. (D) Immunoblot analysis of GFP or endogenous SigmaR1 immunoprecipitates in HEK293T (with or without MG132 treatment), showing Hrd1-mediated SigmaR1 ubiquitination. (E) Immunoblot analysis of Flag immunoprecipitates in HEK293T cells transfected with a combination of plasmids, showing a dose-dependent

interaction between SigmaR1-Flag and Mfn2-EGFP. (F) Immunoblot analysis of Mfn2 oligomers or -containing high molecular weight (HMW) complexes in brown adipocytes treated with or without NE (1 μM, 1 hr) in blue native (BN)-PAGE and regular SDS-PAGE. (G-H) Representative images of mito-DsRed- and mEmerald-Sec61b- expressing pre-adipocytes. DAPI (blue) with quantitation of ER-mitochondrial colocalization using Manders' overlap coefficient (50 cells each) shown in H, one-way ANOVA. (I-J) Confocal images showing the spread and decay of mitochondria-targeted photoactivated GFP (mito-PAGFP) in brown adipocytes 60 min following NE stimulation and photoactivation. Active mitochondrial were stained with TMRE (red). Quantitation of changes of GFP signal intensity over time shown in J. (n=13, 15, and 10 for *Sel1L^{f/f}*, *Sel1L^{−/−}* and *Sel1L ^{−/−};SigmaR1^{−/−}*, one-way ANOVA). All were repeated two to three times. Data are mean ± SEM. **, p< 0.01; ***, p< 0.001.